On the rotation and skew-symmetric forms for incompressible flow simulations

Thomas A. Zang

NASA Langley Research Center, Hampton, VA 23665, USA

Abstract

Zang, T.A., On the rotation and skew-symmetric forms for incompressible flow simulations, Applied Numerical Mathematics 7 (1991) 27-40.

A variety of numerical simulations of transition and turbulence in incompressible flow are presented to compare the commonly used rotation form with the skew-symmetric (and other) forms of the nonlinear terms. The results indicate that the rotation form is much less accurate than the other forms for spectral algorithms which include aliasing errors. For de-aliased methods the difference is minimal.

1. Introduction

The primitive variable form of the three-dimensional incompressible Navier–Stokes equations has several equivalent versions, differing in the precise manner of expressing the nonlinear terms. Among these alternatives are the convection form, $u \cdot \nabla u$, the divergence form, $\nabla \cdot (uu)$, the skew-symmetric form, $\frac{1}{2}u \cdot \nabla u + \frac{1}{2}\nabla \cdot (uu)$, and the rotation form, $\omega \times u + \frac{1}{2}\nabla |u|^2$. (The velocity is denoted by u and $\omega = \nabla \times u$ is the vorticity.) For the past decade the rotation form has been the preferred choice for simulations of transition and turbulence (see [2, Chapter 7]). It has the advantages of favorable conservation properties and economical implementation. However, in his paper, Horiuti [4] exhibited some large-eddy simulations of turbulent channel flow which suggested that the rotation form is markedly less accurate than the skew-symmetric form.

The purpose of the present article is to clarify and to strengthen this conclusion. The calculations presented here are direct simulations (no turbulence modeling), are fully spectral (no low-order finite-difference errors), and encompass simulations of turbulence in homogeneous shear flows as well as of transition in channel and boundary-layer flow. Moreover, some comparisons are made between calculations which include aliasing errors and others in which these errors have been removed.

2. Formulation

The convection form of the incompressible Navier–Stokes equations is

$$\frac{\partial u}{\partial t} + u \cdot \nabla u + \nabla p = \nu \Delta u + S, \tag{1}$$

$$\nabla \cdot u = 0, \tag{2}$$

where S is a source term, the gradient operator,

$$\nabla = \left(\frac{\partial}{\partial x}, \frac{\partial}{\partial y}, \frac{\partial}{\partial z} \right),$$ (3)

and the Laplacian,

$$\Delta = \nabla \cdot \nabla.$$ (4)

The velocity $u = (u_1, u_2, u_3)$, the static pressure is denoted by p, and the kinematic viscosity by ν.

Both spectral Galerkin and spectral collocation methods have been applied to numerical simulations of transition and turbulence. Fourier expansions are used for directions in which periodic boundary conditions are enforced; otherwise, Chebyshev expansions are appropriate. The Galerkin methods are applied in terms of the Fourier–Chebyshev coefficients, whereas the collocation approach is implemented in physical space. The major expense in a Galerkin method is the evaluation of the convolution sums that arise from the nonlinear terms. Transform methods allow this to be done in $O(N \log_2 N)$ operations, where N is the total number of degrees of freedom. Most of the work in a collocation method is absorbed by the approximation of derivatives via analytic differentiation of the spectral interpolant. This, too, requires $O(N \log_2 N)$ operations.

In a proper Galerkin method the convolution sums are evaluated without aliasing errors. This requires the use of the 3/2-rule or of shifted grids in the transform method. A less expensive approach (by about a factor of 2) is the pseudospectral method, in which a more straightforward transform technique is employed at the price of including the aliasing errors.

Similarly, aliasing errors are introduced in the evaluation of the nonlinear terms via a collocation method. They can, however, be eliminated by use of a 2/3-rule, in which the upper third of the frequency spectrum is forced to vanish. Moreover, most Galerkin or pseudospectral methods are algebraically equivalent to some collocaton method, with the 2/3-rule used in de-aliasing for equivalence with the Galerkin method. For simplicity, therefore, the discussion henceforth is confined to (de-aliased) Galerkin methods and to (aliased) collocation methods. We should note that the optimum efficiency—in terms of the minimal number of one-dimensional Fast Fourier Transforms and the minimal storage—can be achieved with the Galerkin formulation [1,12]. The reader is referred to [2, Chapter 7] for the details of spectral methods for the simulation of incompressible flow. Only the most general points have been reviewed here.

The momentum equation in its skew-symmetric form (S) reads

$$\frac{\partial u}{\partial t} + \tfrac{1}{2} u \cdot \nabla u + \tfrac{1}{2} \nabla \cdot (uu) + \nabla p = \nu \Delta u + S.$$ (5)

The term skew-symmetric is used because the operator $\tfrac{1}{2} v \cdot \nabla u + \tfrac{1}{2} \nabla \cdot (vu)$ (for fixed v satisfying $\nabla \cdot v = 0$) is skew-symmetric. Some of the advantages of skew-symmetric operators are discussed in [8,14]. The momentum equation is equivalent to

$$\frac{\partial u}{\partial t} + \omega \times u + \nabla \left(\tfrac{1}{2} |u|^2 \right) + \nabla p = \nu \Delta u + S.$$ (6)

Usually, the static pressure is replaced by the total pressure, $P = p + \tfrac{1}{2} |u|^2$, to produce the customary rotation version (R) of the momentum equation,

$$\frac{\partial u}{\partial t} + \omega \times u + \nabla P = \nu \Delta u + S.$$ (7)

For completeness, we also list here the divergence form (D),

$$\frac{\partial \boldsymbol{u}}{\partial t} + \nabla \cdot (\boldsymbol{uu}) + \nabla p = \nu \Delta \boldsymbol{u} + \boldsymbol{S}, \tag{8}$$

and recall the convection form (C) given in (1).

As discussed in [2, Chapter 2], for Fourier–Galerkin methods the projection (spatial discretization) and differentiation operators commute, but for collocation methods they do not. This means that for the semidiscrete (continuous-in-time, discrete-in-space) momentum equation, the Fourier–Galerkin convection, divergence, and skew-symmetric forms are algebraically identical. Some differences are expected between computations using these forms and those using the rotation form because of the use of the total pressure in the latter. On the other hand, for collocation methods none of these forms are algebraically identical.

Consider now the conservation properties for the ideal inviscid ($\nu = 0$), unforced ($\boldsymbol{S} = 0$), fully periodic case. The ideal Navier–Stokes equations conserve linear momentum, $\int \boldsymbol{u}\, dV$, and kinetic energy, $\int \frac{1}{2} |\boldsymbol{u}|^2\, dV$. For the semidiscrete ideal equations, a Galerkin method conserves the discrete counterparts of both quantities. However, for a collocation method the semidiscrete conservation properties depend upon the exact form of the momentum equation which is discretized. In particular, for the rotation and skew-symmetric forms, both quantities are conserved, for the divergence form only linear momentum is conserved, and for the convection form neither quantity is conserved.

In the presence of physical boundaries, the ideal conservation laws still hold with the boundary fluxes taken into account. However, for the requisite expansions in Chebyshev polynomials the Galerkin projection and differentiation operators do not commute and a semidiscrete conservation law, even accounting for the boundary fluxes, does not hold precisely (see [2, Chapter 4]). Nevertheless, it holds to a sufficient degree of precision to warrant a preference for the conservation form of the semidiscrete equations.

The question of which, if any, of these conservation properties are important for an accurate, physically meaningful simulation is apt to be very problem-dependent. However, the conservation of kinetic energy is virtually mandatory for a simulation to be numerically stable in time. Thus, for quite practical reasons use of the convection or divergence forms is ruled out. Although either of these forms alone is numerically unstable, a method which uses the convection and divergence forms on alternate time steps appears to be well-behaved. We shall refer to this version as the alternating form (A). (Kerr [7] has used an alternating convection–divergence form on a scalar equation appended to the incompressible Navier–Stokes equations in rotation form.)

Only 6 derivatives are required for the evaluation of the nonlinear terms for a collocation approximation in the rotation form, whereas 18 derivatives are needed for the skew-symmetric form. The convection, divergence, and alternating forms take 9 derivatives. (By invoking the incompressibility constraint, the number of derivatives for the convection and skew-symmetric forms can be reduced by 1.) Thus, the rotation form takes the least work for the evaluation of the nonlinear terms, the alternating form slightly more, and the skew-symmetric form appreciably more. Recall, however, that there is additional work required for the pressure and viscous terms. For flows which are inhomogeneous, even in only one direction, the solution of the implicit equations for the pressure and viscous terms takes most of the total CPU time.

3. Homogeneous turbulence

The primary example will be homogeneous turbulence (see Fig. 1), for which the mean flow is $u(x) = (Sy, 0, 0)$, with S denoting the shear rate. This has served as a model problem for many extensive numerical investigations of shear flow turbulence. Numerous references are provided in the review articles by Rogallo and Moin [13] and Hussaini and Zang [6]. Following Rogallo [12], the total velocity is written

$$u = u_0 + u',$$
(9)

and the coordinate transformation,

$$x' = x - Sty, \qquad y' = y,$$
$$z' = z, \qquad\qquad t' = t,$$
(10)

between the Cartesian coordinates (unprimed) and the sheared (primed) coordinates is employed.

The basic equations given in the previous section apply to the primed variables with the source term,

$$S = (-Su_2', 0, 0),$$
(11)

with differentiation with respect to t replaced by differentiation with respect to t', with the gradient operator of (3) replaced by the transformed gradient operator,

$$\nabla' = \left(\frac{\partial}{\partial x'}, \frac{\partial}{\partial y'} - St' \frac{\partial}{\partial x'}, \frac{\partial}{\partial z'} \right),$$
(12)

and with the Laplacian (4) replaced by

$$\Delta' = \nabla' \cdot \nabla'.$$
(13)

The computations are performed in terms of the sheared coordinate system (in which there is a uniform grid) and periodic boundary conditions are enforced in the computational system. As time evolves the physical coordinate system becomes more and more distorted. It has become customary to perform a coordinate re-meshing whenever the angle between the x and y axes reaches $45°$. This is done using

$$x'' = x + y, \qquad y'' = y, \qquad z'' = z.$$
(14)

This re-meshing amounts to rotating the y axis $90°$ in a counterclockwise direction. It is illustrated in Fig. 2. The angle now becomes $135°$ and the computation is continued until it again reaches $45°$. In order to avoid aliasing during the re-meshing, the Fourier modes which alias on a finite grid are removed. These are the modes for which $|k_y - k_x| > \frac{1}{2}N_y$, where N_y is
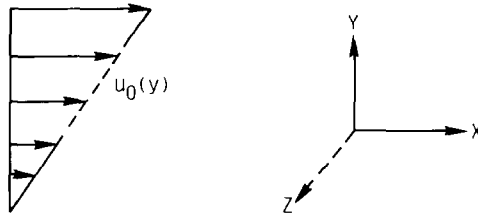

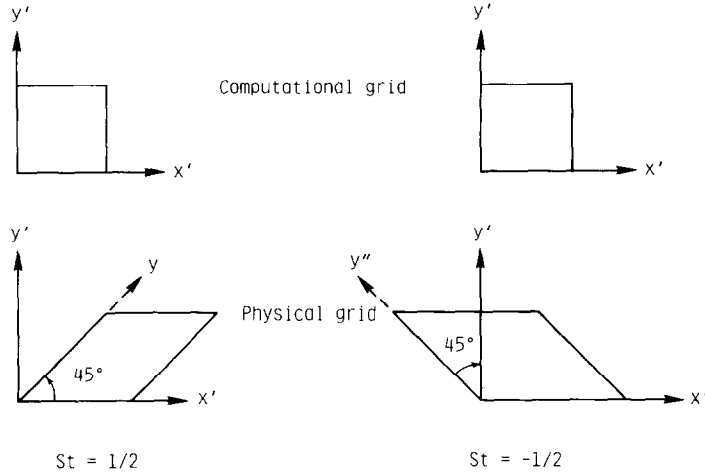Fig. 1. Schematic of the homogeneous, uniform shear problem.

Fig. 2. Physical and sheared (primed) coordinate systems before (unprimed) and after (double primed) re-gridding at $St = \frac{1}{2}$.

the number of grid points in the y direction (see Fig. 3). As a result of this removal of modes, there is a loss of energy during the re-meshing procedure.

The specific uniform shear flow problem chosen here for illustrative purposes has a computational domain of $[0, 2\pi]$ in each coordinate direction, the viscosity $\nu = 0.0212$, and the shear rate $S = 28.3$. The number of grid points in each direction is the same. The time discretization is a low-storage third-order Runge–Kutta method (see [2, Section 4.3.2]) with a time step of roughly half the stability limit.

The initial condition consists of a random divergence-free velocity field whose three-dimensional energy spectrum, $E(k)$, which measures the kinetic energy in a spherical shell in wave number space at a distance k from the origin, satisfies

$$E(k) = \begin{cases} 1, & 12 \leqslant k \leqslant 21, \\ 0, & \text{otherwise.} \end{cases} \qquad (15)$$

The two diagnostics that we shall use in presenting the results of our simulations are the turbulence intensity and the correlation spectra. Let $\langle \cdot \rangle$ denote a spatial average. The turbu-
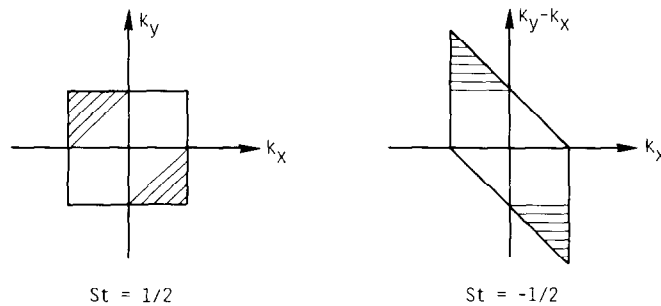

Fig. 3. Wave number transformation at re-gridding. The shaded regions undergo aliasing and are truncated.
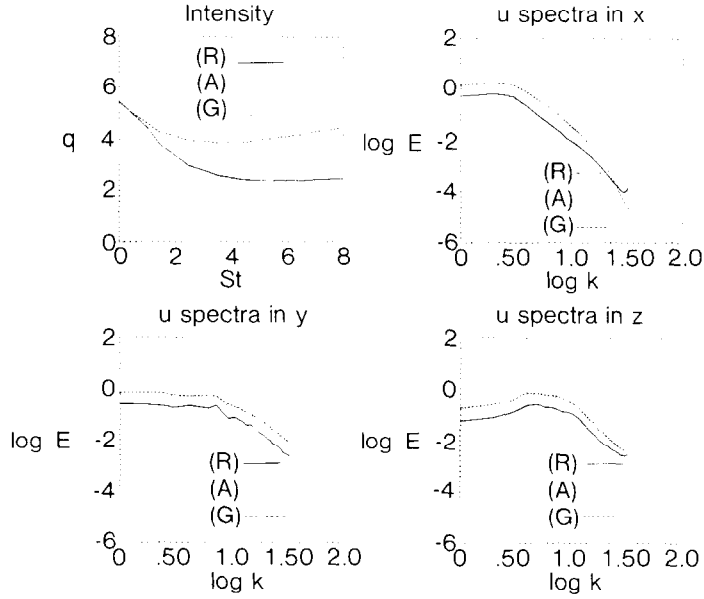
Fig. 4. Rotation (R), alternating (A), and Galerkin (G) results for homogeneous turbulence on a 64^3 grid: turbulence intensity (a) and u auto-correlation spectra in x (b), y (c), and z (d).

lence intensity in the j direction is given by

$$\tilde{u}_j = \langle u'_j(x) u'_j(x) \rangle^{1/2} \tag{16}$$

(no summation on j is intended). The total turbulence intensity is

$$\tilde{q} = \langle \tilde{u}_1^2 + \tilde{u}_2^2 + \tilde{u}_3^2 \rangle^{1/2}. \tag{17}$$

The correlation tensor is given by

$$R_{jk}(r) = \langle u'_j(x) u'_k(x+r) \rangle, \tag{18}$$

and its one-dimensional spectrum in the l direction is

$$E_{jk}(k_l) = \frac{1}{2\pi} \int_0^{2\pi} R_{jk}(r e_l) \, e^{-ik_l r} \, dr, \tag{19}$$

where e_l is a unit vector in the l direction.

Simulations of all the available alternatives have been run for the test problem on a 64^3 grid from a time of $St = 0$ to $St = 8$. Figure 4 displays the results for the rotation, alternating, and Galerkin forms of the nonlinear terms. (The Galerkin calculations used the rotation form.) Figure 4(a) shows the time histories of the total turbulence intensity. The plots were made from measured intensities at intervals of $St = 0.5$. The loss of energy during the re-gridding procedure is quite noticeable here. The most dramatic effect is the inability of the rotation form to sustain the turbulence at the proper level. The alternating form also suffers a slight loss of turbulence intensity, but this is much less than the loss for the rotation form.

Figures 4(b)–(d) give the one-dimensional spectra for E_{11}. Aside from the discrepancy in scale, due to errors in the turbulence intensity, there are differences in shape at the high-wave-number

Table 1
Turbulence properties for 64^3 simulations at $St = 8$

Version	$\bar{q}$	L_{11}	L_{33}	λ_{11}	λ_{33}	S_{11}	S_{33}	F_{11}	F_{33}
rotation	2.4679	0.41607	0.07612	0.32857	0.16547	− 0.45314	0.09365	3.8435	3.4285
alternating	4.2096	0.37039	0.09395	0.30039	0.17161	− 0.84961	− 0.16872	5.0004	3.3062
skew-symmetric	4.2178	0.37165	0.09401	0.30024	0.17154	− 0.85758	− 0.16971	5.0316	3.3025
Galerkin	4.4745	0.38412	0.10144	0.31579	0.17321	− 0.63965	− 0.15038	4.4086	3.2478

end of the spectra. This is most noticeable in the x spectra, primarily because this direction is resolved better than the other two. The aliased results (R and A) have a slower decay than the de-aliased results (G). Although the tails of the aliased results show the familiar curl, this effect is much less pronounced for the alternating form.

Table 1 compares the results at $St = 8$ for several of the 64^3 cases on some specific turbulence properties. The symbols L_{jk} and λ_{jk} denote the integral scale and the microscale, computed by

$$L_{jk} = \frac{1}{\tilde{u}_j^2} \int_0^\pi R_{jj}(re_k)\, dr, \tag{20}$$

and

$$\lambda_{jk} = \tilde{u}_j / \langle (\partial u_j' / \partial x_k)^2 \rangle^{1/2}, \tag{21}$$

respectively. The symbols S_{jk} and F_{jk} refer to the velocity derivative skewness and flatness, which are the third and fourth moments of $\partial u_j' / \partial x_k$, normalized by $\tilde{u}_j^3$ and $\tilde{u}_j^4$, respectively. The difference between the versions of the nonlinear terms increases with the order of the moment involved, and also is greater for quantities involving x-derivatives than those involving z-derivatives. The latter behavior is clearly due to the greater differences in the x spectra. Notice that the (collocation) alternating form results agree quite well with those of the proper skew-symmetric case (and also prove to be numerically stable).

As for the other simulations, the collocation versions of the convection and divergence forms proved to be numerically unstable, whereas the de-aliased computations based on the convection, divergence, and skew-symmetric versions were all numerically stable and the results were indistinguishable. There were slight differences—in the third digit for skewness and flatness and in the fourth digit for the other properties—between these results and those obtained from the de-aliased rotation form. This should be expected since with the fully discrete equations the total pressure is treated implicitly in the latter case, whereas only the static pressure is in the other cases.

A final 64^3 simulation of interest was based on equation (6)—the rotation form using the static rather than the total pressure—using collocation. The results were indistinguishable from those of the standard rotation form.

A similar comparison of three forms of the nonlinear terms is presented in Fig. 5 and Table 2 for simulations on a 96^3 grid. (The initial conditions in Fourier space were identical to those for the 64^3 case.) The same trend is apparent, but the actual differences are less. The rotation form is still unsatisfactory, but now the alternating form is quite acceptable. Figure 6 and Table 3 present corresponding results on a 128^3 grid. (A Galerkin simulation was not conducted here because of the expense involved.) On this grid, even the rotation form now seems acceptable.
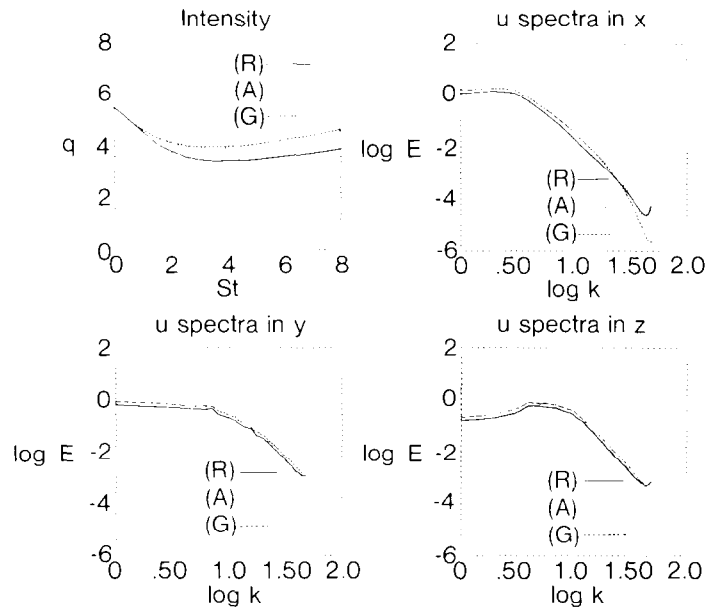
Fig. 5. Rotation (R), alternating (A), and Galerkin (G) results for homogeneous turbulence on a 96^3 grid: turbulence intensity (a) and u auto-correlation spectra in x (b), y (c), and z (d).

Clearly, all the (stable) forms of the momentum equation converge to the same result. However, the absolute error level is much larger for the (collocation) rotation form. Moreover, by the time enough resolution is achieved to resolve the higher-order moments, the collocation alternating form result is just as acceptable as a Galerkin one.
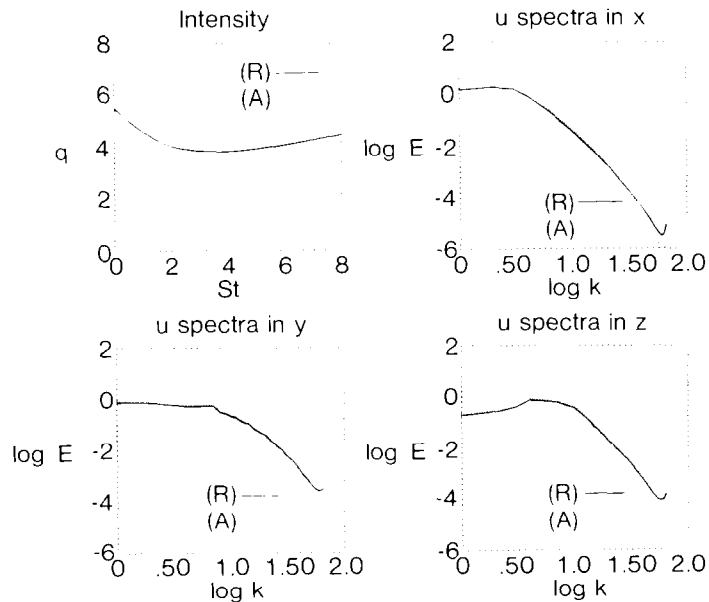

Fig. 6. Rotation (R) and alternating (A) results for homogeneous turbulence on a 128^3 grid: turbulence intensity (a) and u auto-correlation spectra in x (b), y (c) and z (d).

Table 2
Turbulence properties for 96^3 simulations at $St = 8$

Version	$\tilde{q}$	L_{11}	L_{33}	λ_{11}	λ_{33}	S_{11}	S_{33}	F_{11}	F_{33}
rotation	3.8873	0.39110	0.09350	0.32118	0.17371	−0.78180	−0.06726	4.8490	3.5054
alternating	4.5700	0.38979	0.10611	0.30527	0.17216	−0.93917	−0.18593	5.8959	3.3570
Galerkin	4.6246	0.38223	0.10423	0.30875	0.17236	−0.76757	−0.18131	5.0874	3.3483

Table 3
Turbulence properties for 128^3 simulations at $St = 8$

Version	$\tilde{q}$	L_{11}	L_{33}	λ_{11}	λ_{33}	S_{11}	S_{33}	F_{11}	F_{33}
rotation	4.4726	0.38337	0.10362	0.31008	0.17259	−0.83988	−0.16551	5.3763	3.4563
alternating	4.6193	0.37874	0.10359	0.30636	0.17208	−0.91124	−0.19722	5.8916	3.3959

The calculations reported above were performed on a Cray 2. The performance of this machine is heavily dependent upon system load, with timings varying by as much as 30%. On average the timings suggest that the alternating and skew-symmetric form codes took 25% and 50% longer per step, respectively, than the rotation form code. The Galerkin results were obtained with a collocation code using the 2/3-rule on a grid 50% larger in each direction. Although this code produces reduces identical to that of a Galerkin method (see [2, Chapter 3]), it is much less efficient than a highly tuned Galerkin method [12]. Hence timings from this code are not informative.

4. Channel and boundary-layer transition

Another popular application of spectral methods has been to transition in wall-bounded shear flows. The ideal channel flow problem is sketched in Fig. 7. For this problem the source term represents the mean pressure gradient driving the flow and is given by

$$S = (2/\nu, 0, 0). \tag{22}$$

The boundary conditions are no-slip at the walls ($y = \pm 1$), and periodic in x and z. A Fourier
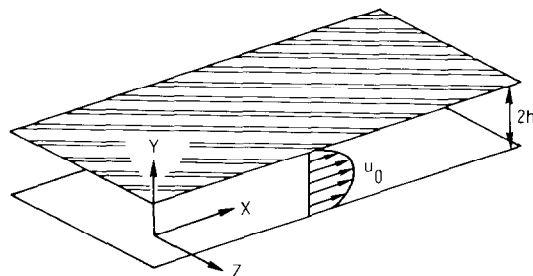

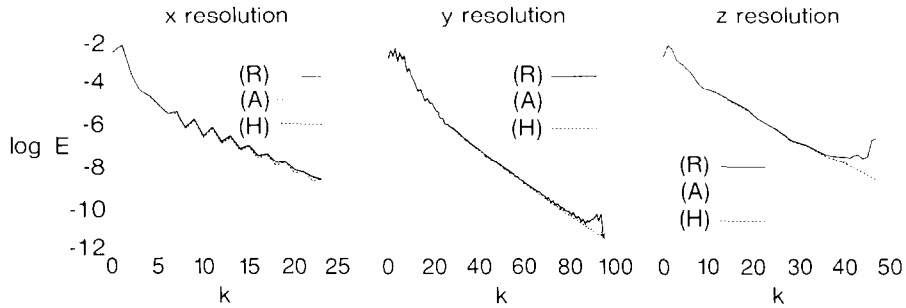Fig. 7. Schematic of the channel flow problem.

Fig. 8. Channel flow resolution spectra at $t = 22.5$ for the rotation (R) form, the alternating (A) form, and a high resolution (H) case.

discretization is used in the two periodic directions and a Chebyshev discretization is used in the direction normal to the wall. Spectral methods for this problem are also covered in depth in [2, Chapter 7]. See [2,6] for detailed references on specific applications.

The particular example that we shall use to illustrate the effect of the form employed for the nonlinear terms in channel flow is the case that has been discussed in great detail by Krist and Zang [9]. The periodicity lengths are 2π in both x and z. The viscosity is $\nu = 1/1500$. The initial conditions at $t = 0$ consist of the mean flow plus prescribed eigenfunctions of the linearized Navier–Stokes equations. The particular spectral method employed for the calculations is the Fourier–Chebyshev collocation scheme described in [15].

The comparison is made over the interval from $t = 15$ to $t = 22.5$ and is restricted to collocation methods. The flow at $t = 15$ is well-resolved (even with the rotation form) on a $48 \times 96 \times 96$ grid. Figure 8 compares the spectra obtained from the rotation and alternating forms at $t = 22.5$. Also included for comparison are the spectra from a high resolution simulation using the rotation form on a $96 \times 128 \times 216$ grid. The results from the alternating form are much closer to those of the high resolution case than are the results from the lower resolution rotation form case. The principal error in the x direction is one of truncation, in the y direction it is one of slight noise at the tail, and in the z direction it is the curl in the tail.

Figure 9 presents some critical flow field features for each of these cases. On the left is shown the vertical shear $(\partial u_1/\partial y)$ in the plane $z = \pi$, which is the so-called "peak plane". On the right is displayed the streamwise vorticity (ω_x) in the plane for which it is most intense $(x = \frac{7}{4}\pi)$. Both flow field features contain strong gradients. On the fine grid, these are resolved sufficiently well. On the coarser grid, the resolution is inadequate, as evidenced by the noticeable oscillations in the flow. These oscillations are much more pronounced for the coarse grid results which used the rotation form than they are for the alternating form case. This is consistent with the spectra and the conclusions of Krist and Zang [9,17], who found that the tails of the spectra need to be roughly 8 orders of magnitude below the level at low wave numbers in order to have sufficient resolution in transition simulations.

Additional simulations indicate that the flow field oscillations are virtually eliminated by a simulation on a $64 \times 96 \times 128$ grid when the alternating form is employed. Equivalent accuracy using the rotation form code required over twice as many total grid points. For the particular channel flow algorithm employed here the alternating form has two additional advantages over the rotation form. The pressure step requires the solution of an implicit equation. This is done
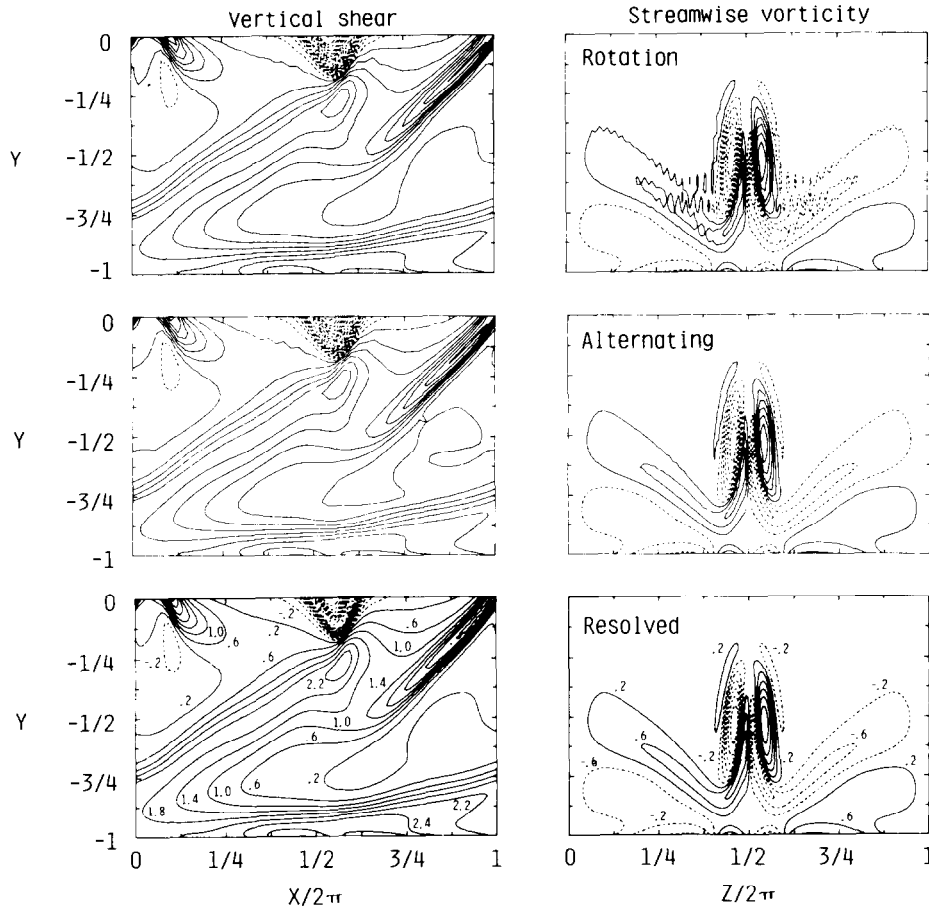
Fig. 9. Vertical shear in the peak plane (left) and streamwise vorticity at $x = \frac{7}{4}\pi$ for channel flow at $t = 22.5$.

with an iterative method. It turned out to take only half as many iterations with the alternating form code as it did with the rotation form code. As a result the overall CPU time for the alternating form code was less than that of the rotation form code. (The bulk of the work in this application occurs in the solution of the implicit equations.) Moreover, the stability limit on the time step (which is governed by the explicit advection limit) is, in practice, over twice as large for the alternating form as for the rotation form code.

Similar improvement is obtained in simulations of boundary-layer transition. The numerical method is the same, with the semi-infinite domain in y handled by an expansion in Chebyshev polynomials in terms of a transformed variable.

A high resolution simulation of boundary-layer transition has recently been performed by Hussaini, Erlebacher and Zang [5,16]. One segment of this simulation (from $t = 4 - 10/80$ to $t = 4 - 14/80$) has been repeated with a calculation using the alternating form instead of the rotation form. Both were performed on a $128 \times 144 \times 288$ grid. A comparison of the resolution spectra at $t = 4 - 14/80$ is provided in Fig. 10. The use of the alternating form has drastically reduced the misbehavior of the tail of the spectra in the y and z directions. These spectra suggest a drastic reduction in the oscillations in the y and z directions but little change in those in the x
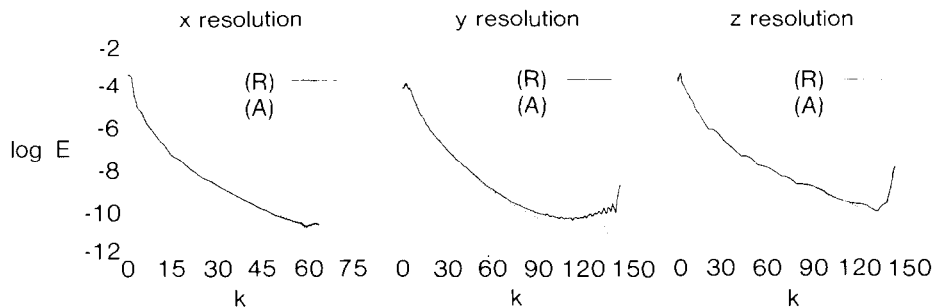
Fig. 10. Boundary-layer resolution spectra at $t = 4 - 14/80$ for the rotation (R) form and the alternating (A) form.
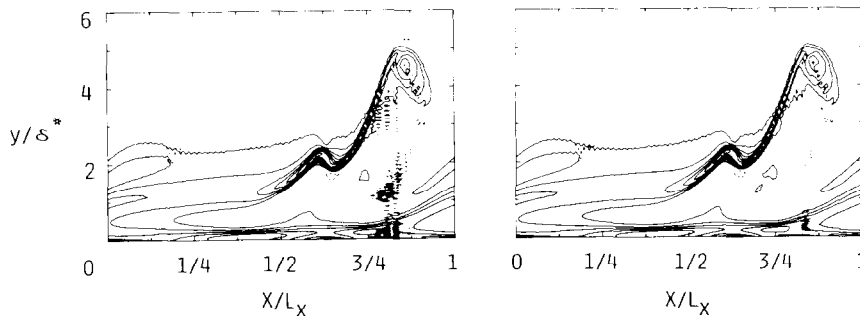

Fig. 11. Vertical shear in the peak plane for boundary-layer flow at $t = 4 - 14/80$: rotation form (left) and alternating form (right).

direction. The improved flow field in the y direction is evident from the reduction in the vertical oscillations in Fig. 11. The oscillations in x have been unaffected, as expected. (Regrettably, data is no longer available to illustrate the reduction in the oscillations in z.)

5. Discussion

The various comparisons presented above reinforce the case raised by Horiuti [4] against the use of the rotation form in numerical simulations of incompressible flow. Since all the computations presented here used fully spectral methods, they enable the cause of the inferior performance of the rotation form to be deduced more clearly than from the calculations of Horiuti who employed low-order finite differences in the y direction. Horiuti found that in his large-eddy simulations of turbulent channel flow (without the use of a residual stress model), the turbulence decayed when the rotation form was employed, whereas it sustained itself under the skew-symmetric form. Faced with the evidence that Moser and Moin [11] had achieved a computation of sustained turbulence in a direct simulation of channel flow using the rotation form, Horiuti concluded, on the basis of some sketchy truncation error analysis, that the errors in the near-wall region were much larger with the rotation form. He speculated that Moser and Moin succeeded because of the greater accuracy of their Chebyshev discretization in the y direction.

The comprehensive results provided in the present paper demonstrate that the blame for the poor performance of the rotation form has been misplaced. All the calculations here were fully

spectral and thus free of the low-order finite-difference errors which Horiuti suspected to be the culprit. Nevertheless, the collocation results based on the rotation form were decidedly inferior to those based on the skew-symmetric (or the more economical alternating) form. And yet, the rotation form performed quite admirably whenever the aliasing errors were removed. Given that Horiuti's calculation included the Fourier aliasing errors, whereas Moser and Moin's employed a Galerkin scheme, the inescapable conclusion is that the rotation form produces aliasing errors that are more damaging than those produced by the skew-symmetric form.

As yet no rigorous demonstration of this property is available. Analysis of the computed flow field for the homogeneous turbulence problem indicates that the root-mean-square aliasing errors for the rotation form are about twice as large as those for the convection, divergence, and skew-symmetric forms. Numerical analysts have proven that aliased and de-aliased spectral algorithms for a variety of nonlinear problems have the same asymptotic rate of error decay as the grid is refined. This includes Fourier spectral methods for homogeneous, isotropic turbulence [10] and Fourier–Chebyshev methods for channel flow [3]. However, these proofs utilized the divergence form. No analysis has been performed for the rotation form. The results in the present paper are consistent with these proofs of convergence. As the grid is refined, all the methods converge to the same solution.

From a practical standpoint, the choice reduces to the skew-symmetric (or alternating) form or any Galerkin method. For spectral methods the final decision rests partly on matters of taste and partly on economics. For finite-difference or finite-element methods, however, the clear choice is the skew-symmetric form. De-aliasing procedures are only available for the simplest grids, and there they add substantially to the cost of the method since the de-aliasing procedure (which uses Fast Fourier Transforms) is much more expensive than the basic discretization.

References

[1] C. Basdevant, Technical improvements for direct numerical simulation of homogeneous three-dimensional turbulence, *J. Comput. Phys.* 50 (1983) 209–214.

[2] C. Canuto, M.Y. Hussaini, A. Quarteroni and T.A. Zang, *Spectral Methods in Fluid Dynamics* (Springer, Berlin, 1988).

[3] C. Canuto and G. Sacchi-Landriani, Analysis of the Kleiser–Schumann method, *Numer. Math.* 50 (1986) 217–243.

[4] K. Horiuti, Comparison of conservative and rotational forms in large eddy simulation of turbulent channel flow, *J. Comput. Phys.* 71 (1987) 343–370.

[5] M.Y. Hussaini, G. Erlebacher and T.A. Zang, Numerical simulations providing a unified view of laminar breakdown in controlled transition experiments (in preparation).

[6] M.Y. Hussaini and T.A. Zang, Spectral methods in fluid dynamics, *Ann. Rev. Fluid Mech.* 19 (1987) 339–367.

[7] R.M. Kerr, Higher-order derivative correlations and the alignment of small-scale structures in isotropic numerical turbulence, *J. Fluid Mech.* 153 (1985) 31–58.

[8] H.-O. Kreiss and J. Oliger, Methods for the approximate solution of time dependent problems, World Meteorological Organization/International Council of Scientific Unions, Geneva (1973).

[9] S.E. Krist and T.A. Zang, Numerical simulation of channel flow transition, NASA TP 2667 (1987).

[10] Y. Maday and A. Quarteroni, Spectral and pseudospectral approximations of Navier–Stokes equations, *SIAM J. Numer. Anal.* 19 (1982) 761–780.

[11] R.D. Moser and P. Moin, The effects of curvature in wall-bounded turbulent flows, *J. Fluid Mech.* 175 (1987) 479–510.

[12] R.S. Rogallo, Numerical experiments in homogeneous turbulence, NASA TM 81315 (1981).

[13] R.S. Rogallo and P. Moin, Numerical simulation of turbulent flows, *Ann. Rev. Fluid Mech.* 16 (1984) 99–137.

[14] E. Tadmor, Skew-selfadjoint form for systems of conservation laws, *J. Math. Anal. Appl.* 103 (1984) 428–442.

[15] T.A. Zang and M.Y. Hussaini, On spectral multigrid methods for the time-dependent Navier–Stokes equations, *Appl. Math. Comput.* 19 (1986) 359–372.

[16] T.A. Zang and M.Y. Hussaini, Numerical simulation of nonlinear interactions in channel and boundary-layer transition, in: R.W. Miksad, T.R. Akylas and T. Herbert, eds., *Nonlinear Wave Interactions in Fluids*, AMD 87 (ASME, New York, 1987) 131–145.

[17] T.A. Zang, S.E. Krist and M.Y. Hussaini, Resolution requirements for numerical simulations of transition, *J. Sci. Comput.* 4 (1989) 197–217.